GEOSCIENCES

Geophysical investigation in sediment cores and its relationship with the governing sedimentary processes at Bransfield Basin, Antarctica

MATEUS DOS SANTOS MARTINS, FABRICIO FERREIRA, ARTHUR AYRES NETO & ROSEMARY VIEIRA

Abstract: This research aims to investigate sediment cores from a glaciomarine environment based on their petrophysical parameters to elucidate lithological and sedimentary issues, as well as to identify a geophysical signature based on their parameter's response. To achieve this objective, six marine sediment cores were collected in the Central Bransfield Basin - Antarctica, the lengths ranging from 1.5 to 5.2 meters in water depths ranging from 304 to 1463 meters. The cores were submitted to different analyses and values from density, magnetic susceptibility, electrical resistivity, p-wave velocity, total gamma radiation, silt, clay and sand contents, and mean grain size for each core location were considered. Four large lithologies were identified according to their geological and geophysical characteristics. The first group is subglacial deformation till (GC16); the second is massive diamicton (GC13 and GC12), the third group is composed of diamictons from the basin (AM10) and lower slope (GC09); the fourth lithological group is composed of siliceous mud from an upper slope location (GC06A). The characteristics recorded across Central Bransfield Basin (from South Shetlands Islands to Antarctic Peninsula) highlighted the relationship between the lithological content and associated depositional processes with the geophysical proprieties as density and magnetic susceptibility.

Key words: Antarctic Peninsula, Glaciomarine environment, petrophysical properties, sediment cores.

INTRODUCTION

The Antarctica Peninsula (AP) is a sensitive area to global climatic and eustatic oscillations (e.g. Garcia et al. 2011, Vaughan et al. 2003). Those climate oscillations were directly reflected in the sedimentary records in different time scales and physiographic provinces, arousing the interest of researchers to understand depositional processes on different scales and areas (Domack & Ishman 1993, Heroy et al. 2008, Khim et al. 2002, Leventer et al. 1996, Yoon et al. 2000).

During the last two decades, the Central Bransfield Basin (CBB) has been the target of geological and geophysical studies, mainly through seismic reflection, to understand the structural evolution of the basin, its formation processes, geometry, and subsurface stratigraphy (e.g. Nobre et al. 2020, Fabrés et al. 2000). In special, the petrophysical, geoacoustic, and geochemical properties of marine sediments are good indicators of the composition, environmental condition, and even the occurrence of past events (e.g. Anderson 1983, Heroy et al. 2008, Rădan et al. 2013, Yoon et al. 1994). The correlation between these data presents potential information for the recognition of distinct sedimentary deposition

processes, sedimentary types and facies, and a key point for the paleoenvironmental reconstructions.

Although knowledge about polar regions has advanced in the past decade, major gaps still exist especially about processes and patterns in glaciomarine environments, and therefore, many valuable aspects remain unresolved. This study aims to investigate and characterize the sediments from Central Bransfield Basin (CBB), Antarctica, considering their geophysical properties and their physiographic province.

Study area

The Bransfield Basin (BB) is a narrow NE-SW oriented submarine basin, located southeast of the South Shetlands Islands (SSI) and the NW of the AP. It is up to 80 km wide and extends over 500 km from Smith Island to Clarence Island. BB is divided into three sub-basins: Western, Central, and Eastern. Due to the sampling effort on site, this work will focus only on the CBB, which is bounded by the elevations of Deception Island and Bridgeman Island (Jeffers et al. 1991).

The CBB is 130 km wide and approximately 230 km long, with a maximum depth of 1950 m and considered highly asymmetric, with a narrow and steep SSI margin to the northwest and a wider, southeastern, AP margin (Ercilla et al. 1998, García et al. 2008, Gràcia et al. 1996, Lawver et al. 1996). CBB is physiographically distinct and can be segmented into continental shelf, slope (upper, middle, and lower), mid-slope platform, basin, and glacial troughs. The continental shelf is up to 50 kilometers wide, with depths between 200 and 300 meters and an inclination of about 1.5°, becoming shallower and narrower in the northeastern direction (García et al. 2008). The SSI margin is narrow, from 6 to 15 km, straight and up to 24° steep. In contrast, the AP margin is wide, from 70 to 85 km, with the break of the smooth platform and slopes generally less than

10° (Prieto et al. 1998). The mid-slope Platform presents an atypical physiographic configuration for a glaciated margin, with a continuous flat surface from the floor of glacial troughs down to the platform edges (García et al. 2009), and consists of the Western platform and the eastern platform. Both have a continuously flat surface (2°) starting from the floor of the glacial troughs and extending to the northeastern basin (García et al. 2011). The ocean basin is relatively narrow and flat, less than 30 km wide. It has four depth levels, which are progressively deeper from 1000 m to 1950 m, from southwest to northeast direction. Glacial troughs in the BB region have irregular longitudinal profiles, becoming shallower towards its central portion and deepening towards the basin in its most distal portions (García et al. 2008). In addition, one of the main characteristics of CBB is the presence of an underwater volcanic chain that was believed to be a result of the volcanism attributed to the rift of the basin (García et al. 2008). Volcanic edifices have different morphologies and can rise above the seabed. Together, they form a discontinuous line that extends from Deception Island to Bridgeman Island.

From an oceanographic perspective, Bransfield Strait can be considered as a transition zone between the Weddell Sea, to the southeast, and the Bellingshausen Sea, to the west (Barker et al. 1998). Its circulation pattern is characterized by the presence of two water masses: one western influx of relatively warm, shallow, less saline, and faster current, Transitional Zonal Water with Bellingshausen influence (TBW) as a result of Gerlache Strait and the Circumpolar Current; and an eastern influx of a colder, deeper, saltier and slower Transitional Zonal Water with Weddell Sea influence (TWW) coming from the Weddell Sea (Sangrà et al. 2011).

MATERIALS AND METHODS

We investigated six sedimentary cores, retrieved across CBB with gravity-corer onboard the Polar Research Vessel Almirante Maximiano (H-41; Brazilian Navy) during the Antarctica Expeditions OPERANTAR XXXIV and XXXV (summers of 2015 and 2016, respectively). The coring sites were located over a 100 km NW-SE transect between the SSI and AP, with depths ranging from 304 m to 1463 m (Fig. 1, Table I). The retrieved cores were sectioned onboard and continuously refrigerated while shipped to Universidade Federal Fluminense (UFF - Niterói/Brazil) for analysis and storage.

Subsequently, to obtain sediment's geophysical parameters as gamma density (g/cm³), p-wave velocity (m/s), electrical resistivity (ohm.m), and magnetic susceptibility ($SI.10^{-5}$), the cores were logged using the Muti-Sensor Core Logger (MSCL; Geotek Ltd.) on a one-centimeter resolution. After MSCL logging, the cores sections were visually described, considering the lithology, color (Munsell 1992), as well as the presence of biological content, sedimentary structures, and rafted debris.

Besides, samples were collected every 5 centimeters along the core. These samples were frozen and lyophilized before applying sodium hexametaphosphate as a deflocculant and finally shaken to break up the particles. Afterward, was applied the granulometric analysis using the particle analyzer Mastersize 2000 (Malvern Instruments). The results were processed based on the Gradistat routine of (Blott & Pye 2001) and sediments were classified according to their sand (%), silt (%), clay (%) contents, and D_{50} values (φ). The Natural gamma spectrometry analyses were performed using the Portable Spectrometer RS-125/230 (GeoRESULTS Pty Ltd), measuring the U (ppm), Th (ppm), K (%), and total gamma radiation (nGy/h). Both analyses,

granulometric and natural gamma spectrometry, were performed on a five-centimeter resolution.

Once this dataset was established, data distribution was analyzed with whisker box-plots, scatter plots, and summary statistic data as mean, median, maximum, and minimum values at Microsoft Statistica 8.0 and Grapher™ 8.0 softwares. Thereby, different lithologies could be classified by their different geophysical properties signature.

RESULTS

Core GC16 SSI (Continental Shelf)

The core GC16 (1.52 m core length; 304 m water depth; Supplementary Material - Table SI) is located at the continental shelf of the SSI margin, between the Robert and Greenwich Islands. The sediments are mainly composed of dominantly Black (GLEY 1 2.5/N) very poorly selected muddy sand. Sediment grain size indicating fine sand, ranging from 2.3 φ at 20 cm below seafloor (BSF) to 4.1 φ at 45 cm BSF (averaging 3.03φ). The sand, silt, and clay content are correlated with the maximum and minimum at 20 cm and 45 cm BSF, showing averages of 64.2%, 31.6%, and 4.2%, respectively (Fig. 2a). The occurrence of shell fragments was recorded at 12 cm BSF, while ice-rafted debris (IRD) were recorded at 72 cm, 80 cm, 91 cm, and 115 cm BSF. The measured density, porosity and p-wave velocity showed minor variation downcore, averaging 1.90 g/cm³, 49%, and 1653 m/s, respectively. A localized decrease in density up to 1.67 g/cm³ at 70 cm followed by a magnetic susceptibility step increase going from 228 $SI.10^{-5}$ (at 46 cm) to 707 $SI.10^{-5}$ at 88 cm BSF. Electrical resistivity and natural gamma data display a relatively uniform profile, averaging 0.60 ohm.m and 209 nGy/h (Fig. 2a, Table SI).
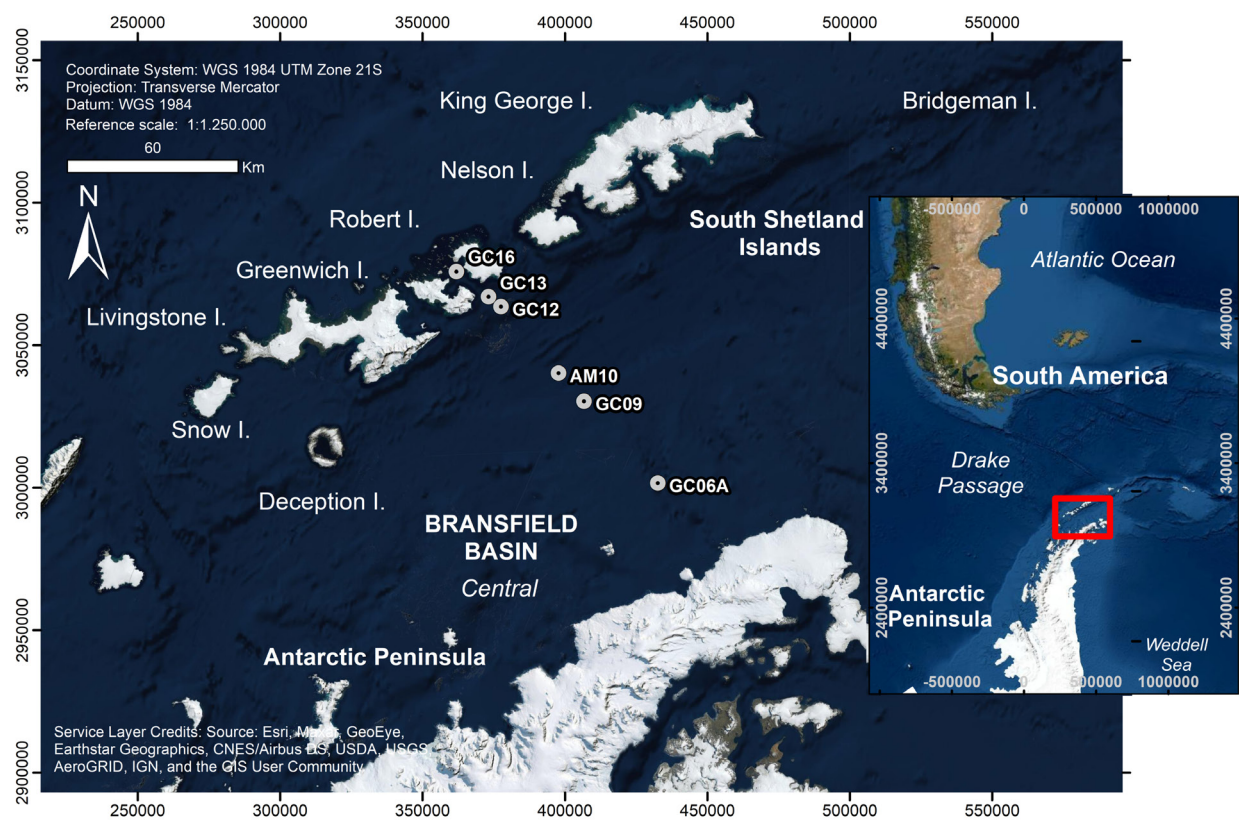
Figure 1. Map of sediment cores location across Central Bransfield Basin (CBB).Cores GC16, GC13 and GC12 located at South Shetlands Islands (ISS) continental shelf and platform and cores AM10, GC09 and GC06A located at basin, Antarctic Peninsula upper and lower platform.

Table I. Locations of the sediment gravity cores studied (located in Fig. 1). Sediment cores have been recovered from different physiographical domains of the Central Bransfield Basin, at depths ranging from 304 m (Continental shelf) to 1463 m (basin).

Depositional environment	Core	Length (m)	Latitude	Longitude	Water Depth (m)
Continental Shelf	GC16	1.52	-59.6740	-62.4234	304
Slope Platform	GC13	4.70	-59.4630	-62.5067	615
	GC12	4.14	-59.3807	-62.5393	760
Basin	AM10	5.20	-59.0015	-62.7545	1463
Lower Slope	GC09	3.35	-58.8328	-62.8454	1022
Upper Slope	GC06A	3.55	-58.3362	-63.1086	840
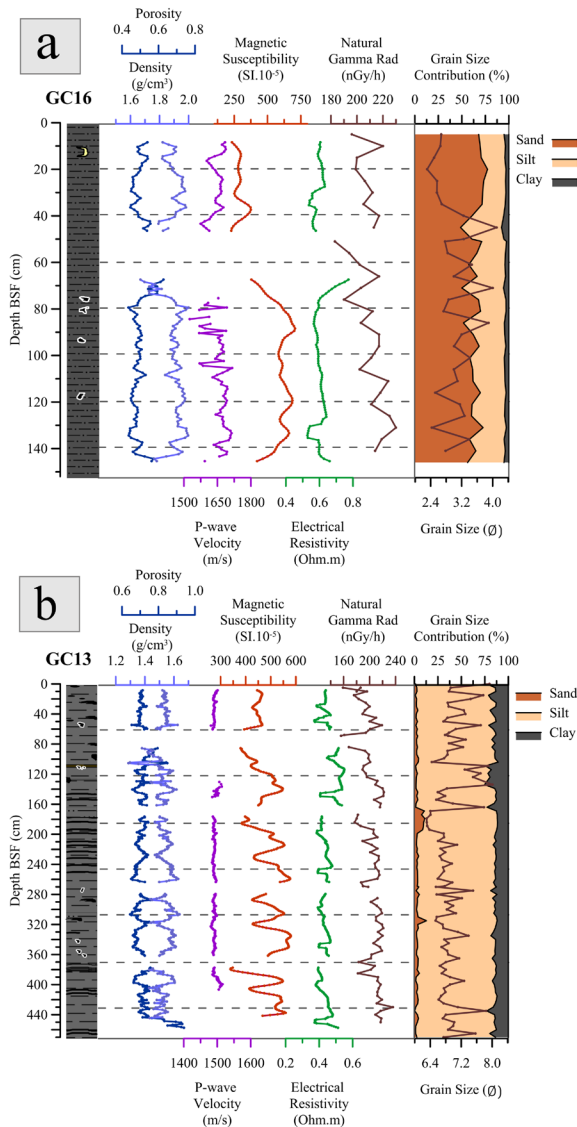
Figure 2. Parameters of density (g/cm³), porosity, p-wave velocity (m/s), magnetic susceptibility (SI.10⁻⁵), electrical resistivity (ohm.m), natural gamma response (nGy/h), granulometric contribution of sand, silt and clay (%) and grain size (φ) plotted in depth BSF profiles. 2a: core GC16. 2b: core GC13.

Cores GC13 and GC12 (SSI Platform)

The cores GC13 (4.70 m core length; 615 m water depth) and GC12 (4.14 m core length; 760 m water depth) (Table I) are positioned at the SSI platform and present similar characteristics. The sediments color is predominantly dark greenish gray (GLEY1 4/10Y) with black (GLEY

1 - 2.5/N) laminations or irregular spots. A massive occurrence of IRD at cores GC13 (50 cm, 110 cm, 275 cm, 340 cm, 360 cm BSF) and GC12 (51 cm, 87 cm, 103 cm, 225 cm, 240 cm, 243 cm, 316 cm, 349 cm BSF) was recorded. Sediment grain size predominantly between 5.90 φ to 8.01 φ (averaging 6.76 φ), which characterizes fine silt. The sand content shows two-step increases at core GC13 (from 200 cm to 175 cm and at 315 cm BSF), and at core GC12 (from 155 cm to 120 cm, and 400 cm to 330 cm BSF), both cores ranging from ~4% to ~12%. Silt and clay content showed averages of approximately 80.0%, and 13.0 %, respectively (Fig. 2b, Table II). Downcore similarities in the acquired MSCL petrophysical properties at cores GC13 and GC12 are observed. Minor variations in density, porosity, p-wave velocity, and electrical resistivity with small peaks throughout the entire core, averaging 1.56 g/cm³, 70%, 1500 m/s and 0.46 ohm.m. Magnetic susceptibility is highly variable with values going from 290 SI.10⁻⁵ to 794 SI.10⁻⁵. Natural gamma response shows an average of 199 nGy/h (Fig. 2b, Table II).

Core AM10 (Basin) and Core GC09 AP (Lower Slope)

The core AM10 (5.20 m core length; 1463 m water depth, Table I) is located at the basin floor of the CBB, close to the volcanic edifices of Three Sisters, and essentially composed of mud, with five layers (up to 3 cm thick) of silty mud/sandy silt with poorly selected sediments. Seven laminations of organic matter (241 cm, 246 cm, 253 cm, 259 cm, 281 cm, 319 cm, 495 cm BSF) and dark greenish gray (GLEY1 4/10Y), greenish-black (GLEY1 3/10Y, GLEY 2.5/10Y), and Olive (5Y 4/2) layers were also recorded (Fig. 3a). The sediments grain size is characterized as fine silt, ranging from 5.92 φ at 510 cm BSF to 7.73 φ at 420 cm BSF (average 6.87 φ). The content of sand, silt, and clay is generally uniform through the

Table II. Summary statistics results from core locations GC13 and GC12, including geophysical and granulometry parameters.

GC13 GC12	P-wave Velocity (m/s)	Density (g/cm³)	Magnetic Susceptibility (SI.10⁻⁵)	Impedance (kg.m⁻²s⁻¹)	Porosity (%)	Electrical Resistivity (ohm.m)	Natural Gamma (nGy/h)
N	575	684	681	567	697	697	161
Min	1481	1.29	290	2131	40%	0.37	156
Max	1529	2.06	794	2961	94%	0.56	237
Mean	1500	1.56	441	2350	70%	0.46	199
Std.dev	9.92	0.06	77	80	4%	0.04	18.23
GC13 GC12	K (%)	U (ppm)	Th (ppm)	φ (D_{50})	Sand (%)	Silt (%)	Clay (%)
N	161	161	161	181	184	184	184
Min	2.8	5.8	25.0	2.78	0.00	0.00	0.00
Max	3.7	17.5	40.1	8.01	64.90	87.57	25.28
Mean	3.3	12.7	32.3	6.76	4.76	80.04	13.57
Std.dev	0.2	2.6	2.8	0.55	6.91	11.85	3.46

core, with an average of 3.2 %, 12.4 %, and 84.4 %, respectively (Fig. 3a).

The core GC09 (3.35 m core length; 1.022 m water depth, Table I) is located at the Antarctic Peninsula lower slope. The sediments are dominated by mud, with intervals of poorly selected silty mud/sandy silt. IRD occurred at 18 cm, 115 cm, 261 cm, and 300 cm BSF. Sediment color are predominant dark greenish gray (GLEY1 4/10Y), with very dark greenish gray (GLEY1 3/5Y and GLEY 2.5/10Y) layers up to 15 cm thick. The sediment grain size is classified as fine silt (averaging 6.06 φ). The amount of silt and clay showed an average of 76.5 % and 10.6 %, respectively, while an increase of sand content was recorded at 237 cm BSF (60.1 %).

Downcore similarities in the acquired MSCL physical properties at cores AM10 and GC09 are also observed. Density, porosity, and p-wave velocity data are relatively uniform with depth, averaging 1.35 g/cm³, 81%, 1528 m/s, respectively. At GC09, a higher peak in the density of 1.62 g/cm³ was registered at 220 cm. Magnetic susceptibility, electrical resistivity and natural gamma response are averaging 103 SI.10⁻⁵, 0.45 ohm.m and 185 nGy/h (Fig. 3a, Table III).

Core GC06A AP (Upper Slope)

The core GC06A (3.35 m core length; 840 m water depth, Table I) is located at the upper slope of AP. The sediments were classified as poorly selected mud, and the occurrence of IRD was recorded at 5 and 10 cm BSF. Several sediment colors patterns were recorded on core GC06A, with dominance of the Olive and Brown (2.5Y - 3/2, 2.5Y - 4/3, 2.5Y - 4/4, 5Y - 5 / 4, 5Y - 4/2, 5Y - 4/3, 5Y - 4/4, 5Y - 4/2, 2.5Y - 3/2). The occurrence of the dark (GLEY1 4/10Y) and very dark greenish gray (GLEY1 3/10Y) were also recorded (between 15 to 0 cm BSF and 205 to 190 cm BSF). A sedimentary gap of about 10 cm thicker was recorded between 146 -136 cm BSF, while gas activity occurs at 285 cm BSF (Fig. 3b, Table SII). Sediment grain size ranging from 4.1 φ (103 cm BSF) to 6.8 φ (5
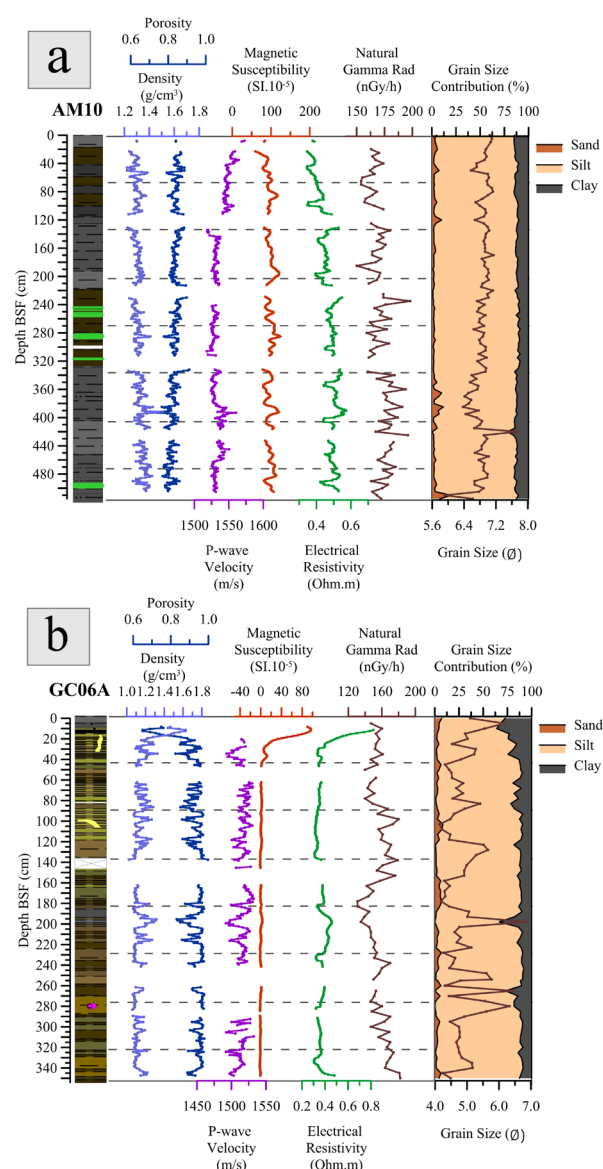
Figure 3. Parameters of density (g/cm³), porosity, p-wave velocity (m/s), magnetic susceptibility (SI.10⁻⁵), electrical resistivity (ohm.m), natural gamma response (nGy/h), granulometric contribution of sand, silt and clay (%) and grain size (φ) plotted in depth BSF profiles. 3a: core AM10. 3b: core GC06A.

cm and 198 cm BSF), and an average of 4.9 φ (coarse silt). The average of sand, silt, and clay was 3.1 %, 82.8 %, and 14.0 %, respectively. The first 25 cm BSF are characterized by higher MSCL parameters values. Density up to 1.63 g/cm³ (65% porosity), magnetic susceptibility up to 97 SI.10⁻⁵, electrical resistivity up to 0.82 ohm.m. However,

below 25 cm BSF, the measured density, porosity, and p-wave velocities are variable throughout the core averaging 1.15 g/cm³, 93%, and 1515 m/s, respectively. Magnetic susceptibility, electrical resistivity, and natural gamma response are uniform, with values averaging 4 SI.10⁻⁵, 0.57 ohm.m, and 158 nGy/h (Fig. 3b, Table SII).

DISCUSSION

Superficial sediments and depositional process at the Central Bransfield Basin

The SSI inner shelf area (core CG16) is characterized by the homogeneous distribution of unselected sands, with chaotically, irregular and size variable fragments dispersed along the core (Fig. 1, Fig. 2a). These sedimentary characteristics support their classification as residual sediments (Anderson 1983), suggesting the predominance of proximal processes associate with glaciers, possibly due to the proximity with the Greenwich and Robert Islands.

During cold intervals (winters and/or glacial periods) the expansion and advance of the ice sheets over the SSI shelf produce severe erosion of the existing sea-floor strata. The eroded material is mainly transported subglacially at the base of ice sheet and deposited at the ice sheet grounding line. However, within the end of cold intervals and beginning of warm intervals (summer and/or interglacial periods), the depositional processes acting on the SSI shelf were mainly characterized by sediment starvation, depositional by-pass and erosion (Prieto et al. 1999). The action of these strong cyclicities characterized by the alternation of the advance and retreat of the glaciers over the SSI shelf associated with the predominance of proximal processes also were supported by the characteristics of the sediment on the studied site area.

Table III. Summary statistics results from core locations AM10 and GC09, including geophysical and granulometry parameters.

AM10 GC09	P-wave Velocity (m/s)	Density (g/cm³)	Magnetic Susceptibility (SI.10⁻⁵)	Impedance (kg.m⁻²s⁻¹)	Porosity (%)	Electrical Resistivity (ohm.m)	Natural Gamma (nGy/h)
N	647	678	680	641	684	672	154
Min	1502	1.21	22	1822	66%	0.34	150
Max	1573	1.62	214	2466	91%	0.57	240
Mean	1528	1.35	103	2061	81%	0.45	185
Std.dev	12.39	0.06	19	84	3%	0.05	21.45
AM10 GC09	K (%)	U (ppm)	Th (ppm)	φ (D_{50})	Sand (%)	Silt (%)	Clay (%)
N	154	154	154	168	170	170	170
Min	2.7	5.9	23.3	3.11	0.00	0.00	0.00
Max	3.7	17.7	38.1	7.73	60.15	89.30	22.08
Mean	3.3	10.9	31.2	6.55	6.87	80.40	11.58
Std.dev	0.2	3.1	2.8	0.50	6.83	10.70	2.29

Residual sediments are recorded at shallower areas, where the drift of icebergs occurs and are strongly influenced by the sea currents that can transport fine sediments (as silt and clay), as well as the poorly selected sand and gravel (Trusel et al. 2010). The proximal environments granulometry is coarser, due to the proximity of source areas with an abundance of basal debris transported by ice (glaciers) and/or on the substrate. Those sediments are deposited as deformation till (Trusel et al. 2010) and, can be formed under the influence of landed glacial margin. In this way, they can end up forming push morainal banks, created by the glacier's advance and retreat process (Rocha-Campos & Santos 2000). In the SSI margin, García et al. (2011) recorded the deposition of the glacially eroded sediments from the archipelago that are transported by the melting water to embankments and basins. The authors describe and classify these sediments as terrestrial mud, and also suggest the possible occurrence of sand horizons associated with those deposits.

The black color recorded over the core should be a result of the sediment composition and geological formation of the SSI, dominated by rocks and sediments of Jurassic-Paleogene volcanic origin (Burton-Johnson & Riley 2015), that had not been verified in previous works.

In the SSI platform (cores GC13 and GC12; Fig. 1; Fig. 2b), the record of poorly selected sediments with low biogenic content supports their classification as massive diamicton, which are characteristic of the transitional glaciomarine sediments (García et al. 2011). Those sediments are also related to the SSI glacial erosion process and delivered towards the slope and basin by the melting water transport of terrestrial mud (with/without sand layers) through the bays, canyons, and associated lobes (García et al. 2011). While, in the lower slope (cores AM10 and GC09; Fig 1. Fig. 3a), our records demonstrated a lithological pattern similar to the massive diamicton, but the higher influence of the oceanic processes appear to act at this area more than in the SSI platform

(cores CG13 and CG12). In the ocean basin, the occurrence of sediments characterized by clayey silt with olive-gray (7.5 Y); olive green (10 Y), and brownish-green (2.5 Y) colors was also recorded close to the AM10 site (Fabrés et al. 2000). The black color layers pattern was also recorded on the SSI platform (core CG13) and AP lower slope (core CG09), suggesting the deposition of volcanic material on those areas (Heroy et al. 2008, Yoon et al. 1994). Occurrences of volcanic material were previously recorded by Yoon et al. (1994) in the BB sediments. The authors describe layers characterized by dark color and composed mostly by well-rounded volcanoclastic material, with fragments of greenish glass and pumice with a smaller amount of terrigenous mineral (less than 40%), suggesting the proximity of the volcanically active regions, as the Three Sisters Island and the Deception Island, as possible source areas.

In the AP upper slope area (core GC06A; Fig. 1; Fig 3b) the sediments are characterized by strongly laminated greenish (2.5Y–4/3) material. Far from proximal environments (SSI and AP margin), the sediment distribution in this area is mainly governed by marine and non-glacial processes (Anderson 1983, Prieto et al. 1998). According to Anderson (1983), these sediments behave like glacial marine sediments, which are better selected and the most abundant in the Antarctic seabed. In addition, the dominance of biological material (mainly diatoms silicate frustules), and the absence of coarser materials (e.g. terrigenous material), also support the suggestion of a restricted input of the terrigenous material on the AP continental shelf and highlight the dominance of biogenic sedimentation process. This sedimentation is characterized by more prominent stratification, better selection, and intense bioturbation (Anderson et al. 1980, Domack et al. 1999). Those characteristics were previously recorded on

the CBB sediments by Yoon et al. (1994), which report the occurrence of well stratified siliceous mud, mainly composed by the diatoms genera *Nitzschia* sp., *Rhizosolenia* sp. and *Chaetoceros* sp. Besides, colored layers (orange to brown-orange) compose mainly by the diatom genera *Chaetoceros* spp. were associated with the annual spring bloom deposition (Leventer et al. 2006). These layers are composed of a set of mixed diatoms with a higher concentration of terrestrial material, which include angular quartz sand, silt, and clay deposited during the summer and autumn seasons. Therefore, well-stratified laminations with a high content of organic matter can be related to the increase of the superficial waters' productivity, resulting in large amounts of biogenic material exported to the seafloor. This increase in the superficial waters productivity occurs in the middle of the CBB, close to the edges of the retracting ice, as a result of melting sea ice, promoting an increase in the stability of the water column (Jordan & Pudsey 1992, Smith & Nelson 1985), and responsible for the large amounts of biogenic material in a short period, allowing the mass sedimentation of diatom frustules (Honjo et al. 1982, Smith & Nelson 1985). The laminations of organic material (diatomaceous mud) were also recorded on isolated depths of the AP lower slope, at core AM10 (Fig. 3a), indicating the predominance of biogenic sedimentation in open-marine conditions (pelagic and hemipelagic sediments) during short periods, as the spring and/or summer blooms (Fabrés et al. 2000, Heroy et al. 2008, Milliken et al. 2009).

The presence of IRD on marine sedimentary cores indicates that icebergs, sea ice, and mass-flow processes (e.g. turbidity and debris flow processes), and/or all those processes acting in the region during a known time interval (Anderson 1999, Yoon et al. 1997, Cofaigh et al. 2001). The type of rock in the debris can be used

to identify the source area of the iceberg. Even in the modern age, under exceptional conditions, icebergs can spread far beyond their normal limits, so this interpretation must be cautious. The IRD recorded in the SSI continental margin (core GC16) and platform (cores GC13 and GC12), and in the AP lower slope (core GC09) and upper slope (core GC06A) suggest the contribution of the debris transported by icebergs and mass-flow processes to the central area of the CBB during the warmer periods, as recorded by (Yoon et al. 1997) at Admiralty Bay. These glaciogenic particles were not recorded at the lower slope, represented by core AM10, our deeper location, indicating the absence of iceberg discharge and mass-flow processes on the core site, and the dominance of oceanographic processes acting as the main depositional controller.

So far, there is no general scheme by which bioturbations can be categorized in glacial marine sediments. The bioturbation recorded in cores GC16 and GC06A results from the disturbance of sediments caused by benthic animals crawling on the seabed or, when in the subsurface, for reasons of habitation or feeding. Infauna activity is limited by the oxidation status of the bottom waters, the amount of organic matter in the sediment, and the redox potential of the porous fluid (Domack & Powell 2018). Bioturbation mixes the primary depositional signal (Anderson 2001) and, therefore, documentation is important to assess whether proxy data can be useful in the case of non-laminated sediments. During the process of anaerobic degradation of organic compounds, carried out by bacteria and other microorganisms methane and carbon dioxide are produced. Boyd et al. (2010) have already shown methanogenesis in subglacial sediments through an active population of organisms associated with subglacial sediments from Robertson Glacier, in the Canadian Rockies. Thus, considering the GC06A core as composed

of diatoms (siliceous mud and oozes), the presence of gas at 285 cm may be the result of the methanogenesis process, due to the high productivity in the spring and summer months (Hagen & Vogt 1999, Heroy et al. 2008, Winfrey & Zeikus 1977).

Petrophysical properties of glaciomarine sediments

The petrophysical characteristics of the marine sediments recovered from the CBB presented distinct profiles, reflecting the complexity of sedimentary sources, transport mechanisms, and rework actions that occur at each site location. Looking at each parameter individually, it is possible to see that sediment density decreases towards the AP. The lithologies identified as tills presented higher densities, followed by diamictons, with the lowest values being associated with siliceous mud. Except for values associated with IRD, the density display values between 1.9 and 2.0 g/cm^3 for tills, from 1.3 to 1.8 g/cm^3 for diamicton, and 1,1 to 1.3 g/cm^3 for siliceous mud. These values are in agreement with the data compilation presented by Wohlenberg (1982). The author identified the density for unconsolidated sediments ranging from 2.0 to 2.7 g/cm^3 for clays and 1.4 to 1.9 g/cm^3 for organic clays. These patterns were also recorded by García et al. (2011) that found similar results for CBB and with the sediment density presented for Marshall (1975) that ranges around 1.4 g/cm^3 in clay and 1.2 g/cm^3 in siliceous mud.

The oscillation on the p-wave velocity of the CBB sediments was, in general, distinct between the SSI continental shelf (core GC16) and the other locations, showing a good agreement with density. The large fluctuations recorded can reflect the changes in the granulometry. This suggestion is supported by the p-wave velocity analysis carried out at the continental shelf from the northern Pacific Ocean by Hamilton
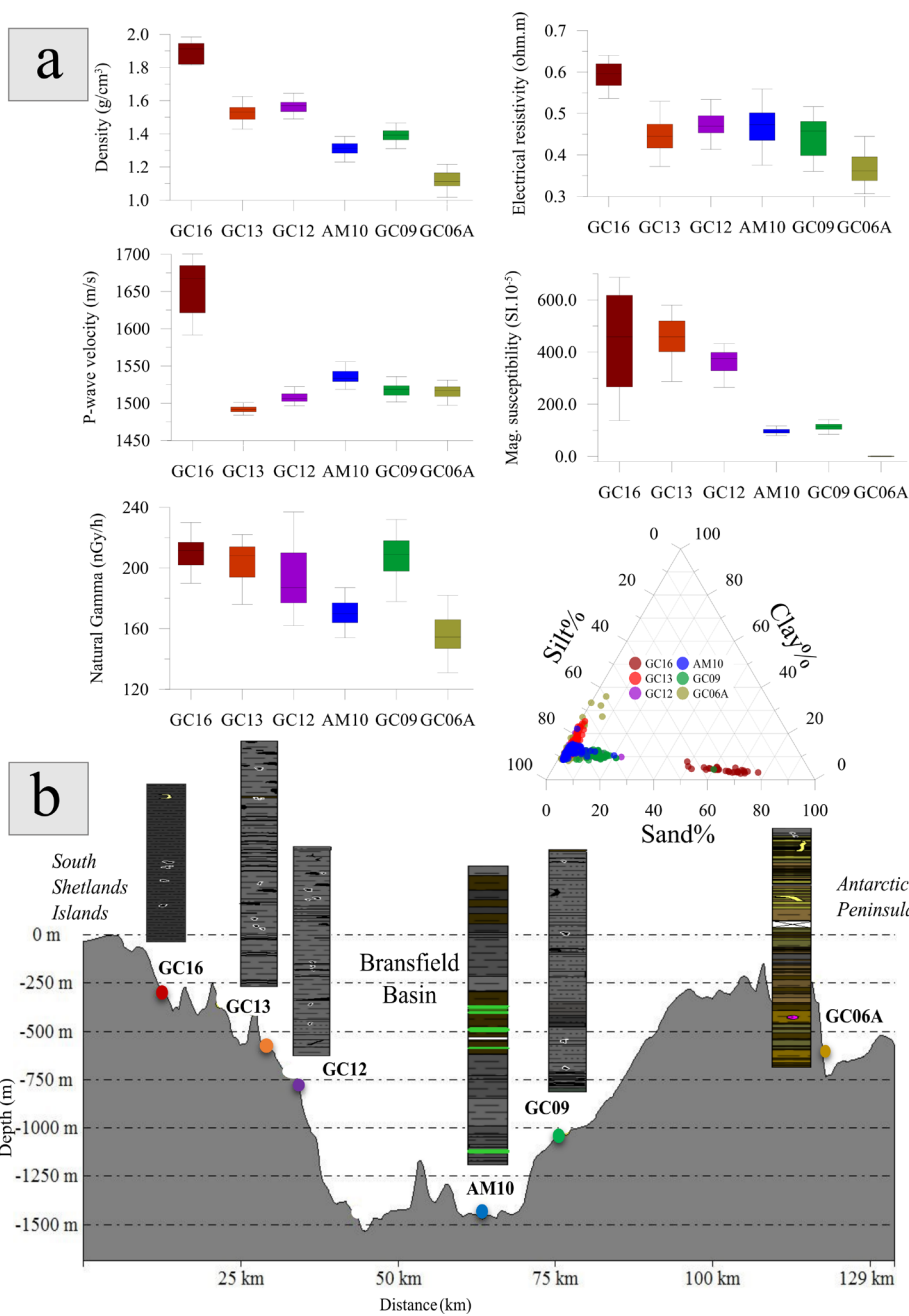
Figure 4. 4a: Box-whisker plots for geophysical properties per core location considering minimum, maximum, median, lower quartile, and upper quartile for groups of data and ternary diagram comparing the relative (%) sand/silt/clay grain sizes fractions for the six studied cores. 4b: Bathymetric profile with sediment core location and description at Central Bransfield Basin.

(1980), which revealed an increase in the velocity of the compressional wave as a function of the increase in grain size. In this study, the coarse sands showed higher speeds, reaching 1836 m/s, when compared to finer sediments (1520 m/s in silty clays to 1646 m/s in silty sand), while the geoacoustic parameters are mainly influenced by the type of fluid present in the porous space. Gases are more compressible than liquids, so p-wave values are lower in gas-filled sediments. Thus, the presence of gas very possibly came to contribute to anomalies and consequently the absence of p-wave data (between 250 and 300 cm) recorded on core GC06A. The p-wave velocity in unconsolidated sediments is relatively uniform, between 1500 to 1600 m/s in siliceous oozes and even in clays (Marshall 1975). Sediments from Deception Island already

studied by (Leitão et al. 2016) presented values between 1532 m/s and 1564 m/s for fine silts.

In marine sediments, magnetic susceptibility can vary from the absolute minimum value of -1.5 SI.10^{-5} (diamagnetic minerals, such as pure calcite or quartz) to a maximum of 1000 SI.10^{-5} for basaltic debris rich in (titanium) magnetite (Bleil et al. 1996). That means the fluctuations in magnetic susceptibility can be interpreted by a higher iron content or, more generally, by a large amount of magnetic particles within a given volume. In this way, the highest values recorded near the SSI, linked to the tills and diamicton can be associated with the SSI geological matrix, due to the proximity with the Greenwich and Robert Islands, Three Sisters volcanic pinnacles formation, or even by debris transported from Deception Island, which is an active volcano (Burton-Johnson & Riley 2015). Distant locations from SSI, as diamicton and siliceous mud, possibly have a greater contribution of the AP rock matrix, composed mainly by sedimentary rocks (Burton-Johnson & Riley 2015), besides biogenic material, indicating sediments rich in silica, carbonates, and/or organic matter (Heroy et al. 2008). Previous studies show magnetic susceptibility values below to our records for different regions of the world, as at cores from lakes near the Black Sea, where values of magnetic susceptibility between 0 and 45 SI.10^{-5} were used as proxies for a lithological description of detritic material, organic matter and carbonates (Radan et al. 2013). Magnetic susceptibility measurements on the Amazon Platform also show constant values around 10 SI.10^{-5}, with high intensities reaching 42.7 SI.10^{-5} (Bleil et al. 1996). According to the authors, the average value for clayey soils was 70 SI.10^{-5}, and for mixed texture it was 45 SI.10^{-5}, both measured between 0.2 and 0.4 m BSF. In Frobisher Bay in Canada, Andrews & Stravers (1993) studied the glacial environment where the medians values

(per core analyzed) ranged from 6 to 709 SI.10^{-5} agree with our records in the CBB.

The electrical resistivity does not show significant variations. However, lower values are found towards AP (core GC06A; 0.37 ohm.m; Fig. 3b; Table SII) as well as density and magnetic susceptibility parameters, probably caused by the saturation and salinity inside the pores. The electrical resistivity of water-saturated sediments depends on the sum of the resistivity of their solid and fluid portions. Since silicate grains are poor conductors, an electric current spread mainly in the fluid within the pore. Therefore, according to Schulz & Zabel (2013), the dominant transport mechanism of the electric current is electrolytic conduction of ions and molecules with excess or deficiency of electrons. According to this, the predominant water mass in the CBB and their different salinity patterns (TBW and TWW) may be influencing the electrical resistivity measured within the sediments.

The total natural gamma radiation in CBB sediments showed considerable variations. The high gamma-ray response indicates the presence of clay-rich deposits, such as shale, claystone, while relatively low gamma radiation indicates the presence of coarse-grained sandstone or carbonate rocks (Klaja & Dudek 2016). However, our data suggest that the natural radiation in CBB is mainly controlled by the Uranium content, with Thorium participation, and with a poor Potassium contribution, as widely discussed by Nobre et al. (2020) with the same dataset. As the lithologies classification, uranium levels present a slight decrease towards the AP. The highest mean value of U was found in SSI continental shelf (core GC16; 14.4ppm), while the lowest occurs at AP upper slope (core GC06A; 7.4ppm). The intermediate locations presented average values between 8.9ppm and 13.9ppm. Nobre et al. (2020) also suggested that sediment core distance from AP reflects the distribution

of gamma-ray content at CBB sediments when analyzed by its proportion in terms of U/K and Th/U, resulting in higher contribution of thorium in sediments near to ISS and higher contribution of uranium in the deeper and distal cores locations, due to preservation of organic matter.

This relationship corroborates with the water content, which, as demonstrated by Klaja & Dudek (2016), tends to present an inverse correlation with total natural gamma radiation. The total amount of uranium measured by the spectrometer includes both detrital and authigenic contributions of uranium. Due to the solubility of the uranium in water when under oxidizing conditions, uranium can be partially transported in the form of Uranyl carbonate complexes (Bodin et al. 2011). Therefore, an increase in the amount of authigenic Uranium may indicate a depositional environment with oxygen depletion (Wignall & Myers 1988). Hassan et al. (1976) showed a strong correlation between the U content and the organic carbon and organic matter content. Uranium species can be adsorbed on clay minerals or associated with accessory minerals and on colloidal Fe oxide/hydroxide coatings, of the mineral grains. Thorium is commonly concentrated in residual terrigenous deposits, such as bauxite and clay due to be practically insolubility (Hassan et al. 1976). Important amounts of thorium are recorded in heavy minerals such as monazite, rutile, and zircon. Hassan et al. (1976) reported a correlation between the Th and clay mineral content. However, the authors have not proven that the clays were responsible for the Th enrichment. Considering the spectral proportions, the CBB sediments can be composed of illite, since their typical potassium levels are around 3% (Nielsen et al. 1987). According to Kühnel (1996), illite is a clay mineral characteristic of a cold climate.

Density and Magnetic Susceptibility signature

The geological and petrophysical characteristics recorded across the CBB (from SSI to AP) highlighted the relationship between the lithological content and associated depositional processes with the geophysical proprieties as density and magnetic susceptibility (Fig. 5a). In general terms, both geophysical proprieties (density and magnetic susceptibility) presented higher values as well near the SSI that decreases towards the AP (Fig. 4, Table VI).

Our records support that those distinct petrophysical ranges recognized through the site locations present a close relationship with the local lithologies, depositional process, and distance of sediments source areas. The highest petrophysical values are associated with lithologies classified as deformation tills from the SSI continental shelf (core GC16; average density 1.90 g/cm^3; average MS 497.41 SI.10^{-5}; Fig. 4, Table IV), followed by the diamictons from the SSI platform (cores GC13 and GC12; average density 1.56 g/cm^3; average MS 440.8 SI.10^{-5}; Fig. 4, Table IV), while the diamictons from the AP lower slope (cores AM10 and GC09; average density 1.35 g/cm^3; average MS 102.7 SI.10^{-5}; Table IV) and de siliceous mud from the AP upper slope (core GC06A (average density 1.15 g/cm^3; average MS 4.3 SI.10^{-5}; Fig. 4, Table IV) presents lower values. In this way, the highest values recorded in the SSI site locations are directly associated with the geological matrix of the area. The SSI continental shelf and platform present a geological matrix related to the faster glaciers decay during the warmer conditions (due to their relative small drainage area), that associated with the strong cyclicity of the advance and retreat of the glaciers, easily eroded volcaniclastic source and the high rates of meltwater production, that promote the basinward transport of a large volume of sediments, mainly by meltwater plumes and mass-gravity flows, as slumps, turbidity currents
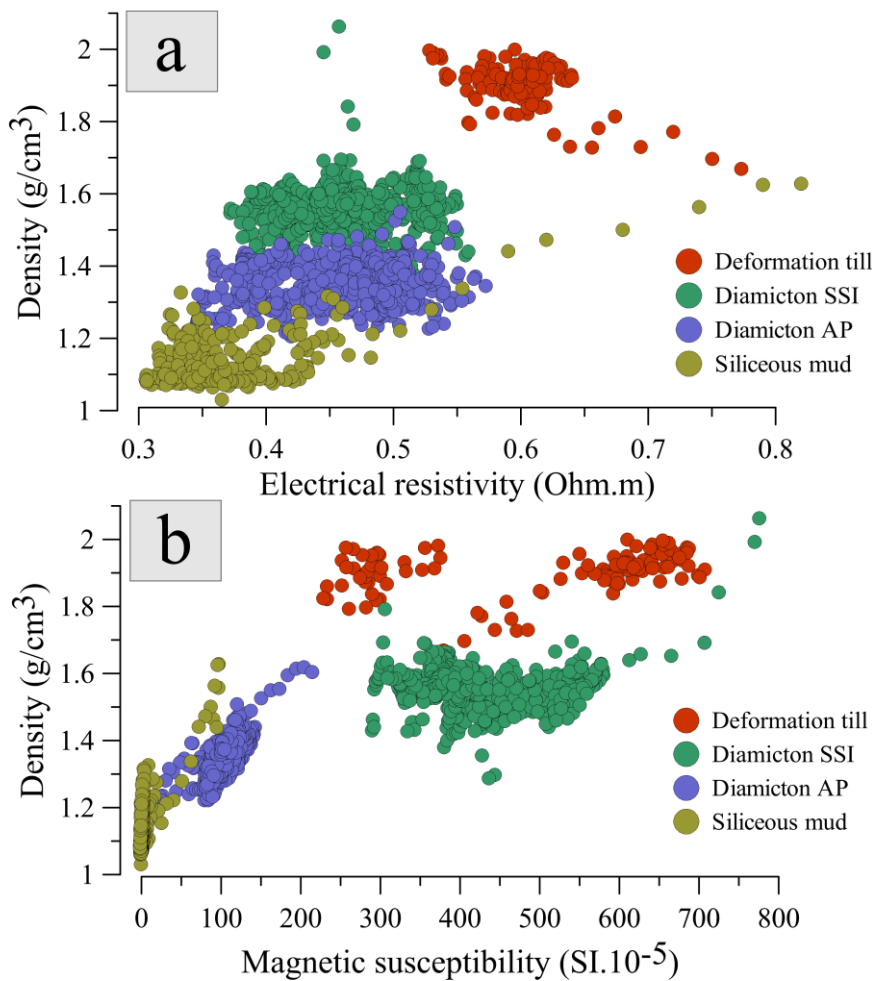
Figure 5. 5a: Class scatter plot of density (g/cm3) and magnetic susceptibility (SI.10-5) according with lithology of deformation till, diamiction (near SSI or AP) and siliceous mud. 5b: Class scatter plot of density (g/cm3) and electrical resistivity (ohm.m) according with lithology of deformation till, diamiction (near SSI or AP) and siliceous mud.

and gravitational instabilities (Prieto et al. 1999). In addition, other volcanic source areas as the Three Sisters volcanic pinnacles formation, or even by debris transported from Deception Island, can also contribute to the increase observed in the petrophysical properties (Burton-Johnson & Riley 2015).

However, in the site locations distant from SSI, as the AP diamicton and siliceous mud (cores AM10, GC09, and GC06A), the higher contribution of the AP rock matrix, composed mainly by sedimentary rocks (Burton-Johnson & Riley 2015), besides biogenic material, indicating sediments rich in silica, carbonates, and/or

organic matter, with the low influence of volcanic material.

CONCLUSIONS

Four large lithological groups can be identified according to their geological and petrophysical characteristics, especially by their magnetic susceptibility and density data. The first group consists of subglacial deformation till (GC16), which presented the color black (GLEY 1 2.5 / N), higher values of density (1.90 g/cm^3) magnetic susceptibility (497 SI.10^{-5}), p-wave (1653 m/s) and grain size (3.02φ); the second and third group corresponds to massive diamicton from South

Table IV. Mean values of geophysical parameters and granulometry data by their respective lithology and physiographic environment.

Physiographic environment		Lithology	P-wave Vel. (m/s)	Dens. (g/cm^3)	Mag. Susc. (SI.10^{-5})	Elec. Resis. (ohm.m)	φ (D$_{50}$)
Continental Shelf	SSI	Deformation Till	1653	1.90	497	0.60	3.02
Slope Platform	SSI	Massive diamicton	1500	1.56	441	0.46	6.76
Basin Lower / Slope	AP	Massive diamicton	1528	1.35	103	0.45	6.55
Upper Slope	AP	Siliceous mud	1515	1.15	4	0.37	4.92

Shetlands Islands (GC13 and GC12), basin (AM10) and lower slope (GC09), variable gray color and intermediate values of density, magnetic susceptibility, and p-wave velocity; the fourth lithological group is composed of siliceous mud from an upper slope location (GC06A) presenting an olive/brown color and gas detection, with lower values for density (1.15 g/cm^3), magnetic susceptibility (4 SI.10^{-5}), electrical resistivity (0.37 ohm.m) and natural gamma response (158 nGy/h).These values can be used on further research.

Acknowledgments

REFERENCES

ANDERSON DM. 2001. Attenuation of Millennial-Scale Events by Bioturbation in Marine Sediments. Paleoceanogr Paleoclimatol 16(4): 352-357. doi: 10.1029/2000PA000530.

ANDERSON JB. 1983. Ancient Glacial-Marine Deposits: Their Spatial and Temporal Distribution. In Glacial-Marine Sedimentation. Springer, p. 3-92.

ANDERSON JB. 1999. Antarctic Marine Geology. Cambridge University Press, p. 58-88. doi: 10.1017/CBO9780511759376.

ANDERSON JB, KURTZ DD, DOMACK EW & BALSHAW KM. 1980. Glacial and Glacial Marine Sediments on the Antarctic Continental Shelf. J Geol 88(4): 399-414. doi: 10.1086/628524.

ANDREWS JT & STRAVERS JA. 1993. Magnetic Susceptibility of Late Quaternary Marine Sediments, Frobisher Bay, NWT: An Indicator of Changes in Provenance and Processes. Quat Sci Rev 12(3): 157-167. doi: 10.1016/0277-3791(93)90050-V.

BARKER PF, BARRETT PJ, CAMERLENGHI A, COOPER AK, DAVEY FJ, DOMACK EW, ESCUTIA C, KRISTOFFERSEN Y & O'BRIEN PE. 1998. Ice Sheet History from Antarctic Continental Margin Sediments: The ANTOSTRAT Approach. Terra Antarctica 5(4): 737-760.

BLEIL U ET AL. 1996. Report and Preliminary Results of Meteor Cruise 34/1 Cape Town-Walvis Bay, 03.01. 1996-26. 01. Berichte Aus Dem Fach Bereich Geowissenschaften, Universität Bremen 77.

BLOTT SJ & PYE K. 2001. Gradistat: A Grain Size Distribution and Statistics Package for the Analysis of Unconsolidated Sediments. Earth Surf Process Landf 26(11): 1237-1248. doi: 10.1002/esp.261.

BODIN S, FRÖHLICH S, BOUTIB L, LAHSINI S & REDFERN J. 2011. Early Toarcian Source-Rock Potential in the Central High Atlas Basin (Central Morocco): Regional Distribution and Depositional Model. J Pet Geol 34(4): 345-363. doi: 10.1111/j.1747-5457.2011.00509.x.

BOYD ES, SKIDMORE M, MITCHELL AC, BAKERMANS C & PETERS JW. 2010. Methanogenesis in Subglacial Sediments. Environ Microbiol Rep 2(5): 685-692. doi: 10.1111/j.1758-2229.2010.00162.x.

BURTON-JOHNSON A & RILEY TR. 2015. Autochthonous v. Accreted Terrane Development of Continental Margins: A Revised in Situ Tectonic History of the Antarctic

Peninsula. J Geol Soc 172(6): 822-835. doi: 10.1144/jgs2014-110.

COFAIGH CO, DOWDESWELL JA & PUDSEY CJ. 2001. Late Quaternary Iceberg Rafting along the Antarctic Peninsula Continental Rise and in the Weddell and Scotia Seas. Quat Res 56(3): 308-321. doi: 10.1006/qres.2001.2267.

DOMACK EW & ISHMAN S. 1993. Oceanographic and Physiographic Controls on Modern Sedimentation within Antarctic Fjords. GSA Bulletin 105(9): 1175-1189. doi: 10.1130/0016-7606(1993)105<1175:OAPCOM>2.3.CO;2.

DOMACK EW, JACOBSON EA, SHIPP S & ANDERSON JB. 1999. Late Pleistocene-Holocene Retreat of the West Antarctic Ice-Sheet System in the Ross Sea: Part 2 - Sedimentologic and Stratigraphic Signature. GSA Bulletin 111(10). doi: 10.1130/0016-7606(1999)111<1517:lphrot>2.3.co;2.

DOMACK EW & POWELL R. 2018. Modern Glaciomarine Environments and Sediments. In Past Glacial Environments. Elsevier, p. 181-272. doi: 10.1016/B978-0-08-100524-8.00030-0.

ERCILLA G, BARAZA J, ALONSO B & CANALS M. 1998. Recent Geological Processes in the Central Bransfield Basin (Western Antarctic Peninsula). Geol Soc Spec Publ 129(1): 205-216. doi: 10.1144/GSL.SP.1998.129.01.13.

FABRÉS J, CALAFAT A, CANALS M, BÁRCENA MA & FLORES JA. 2000. Bransfield Basin Fine-Grained Sediments: Late-Holocene Sedimentary Processes and Antarctic Oceanographic Conditions. The Holocene 10(6): 703-718. doi: 10.1191/09596830094953.

GARCÍA M, ERCILLA G & ALONSO B. 2009. Morphology and sedimentary systems in the Central Bransfield Basin, Antarctic Peninsula: sedimentary dynamics from shelf to basin. Basin Res 21(3): 295-314. doi: 10.1111/j.1365-2117.2008.00386.x.

GARCÍA M, ERCILLA G, ALONSO B, CASAS D & DOWDESWELL JA. 2011. Sediment Lithofacies, Processes and Sedimentary Models in the Central Bransfield Basin, Antarctic Peninsula, since the Last Glacial Maximum. Mar Geol 290(1-4): 1-16. doi: 10.1016/j.margeo.2011.10.006.

GARCÍA M, ERCILLA G, ANDERSON JB & ALONSO B. 2008. New Insights on the Post-Rift Seismic Stratigraphic Architecture and Sedimentary Evolution of the Antarctic Peninsula Margin (Central Bransfield Basin). Mar Geol 251(3-4): 167-182. doi: 10.1016/j.margeo.2008.02.006.

GRÀCIA E, CANALS M, FARRÀN ML, PRIETO MJ, SORRIBAS J & TEAM G. 1996. Morphostructure and Evolution of the Central and Eastern Bransfield Basins (NW Antarctic Peninsula). Mar Geophys Res 18(2): 429-448. doi: 10.1007/bf00286088.

HAGEN RA & VOGT PR. 1999. Seasonal Variability of Shallow Biogenic Gas in Chesapeake Bay. Mar Geol 158(1-4): 75-88. doi: 10.1016/S0025-3227(98)00185-6.

HAMILTON EL. 1980. Geoacoustic Modeling of the Sea Floor. J Acoust Soc Am 68(5): 1313-1340.

HASSAN M, HOSSIN A & COMBAZ A. 1976. Fundamentals of the Differential Gamma Ray Log-Interpretation Technique. In SPWLA 17th Annual Logging Symposium. Society of Petrophysicists and Well-Log Analysts.

HEROY DC, SJUNNESKOG C & ANDERSON JB. 2008. Holocene Climate Change in the Bransfield Basin, Antarctic Peninsula: Evidence from Sediment and Diatom Analysis. Antarct Sci 20(1): 69-87. doi: 10.1017/S0954102007000788.

HONJO S, MANGANINI SJ & POPPE LJ. 1982. Sedimentation of Lithogenic Particles in the Deep Ocean. Mar Geol 50(3): 199-220. doi: 10.1016/0025-3227(82)90139-6.

JEFFERS JD, ANDERSON JB & LAWVER LA. 1991. Geological Evolution of Antarctica. In Evolution of the Bransfield basin, Antarctic Peninsula. Thompson, M.R.A., Crame, J.A., Thomson, J.W. Cambridge Univ. Press, Cambridge, p. 481-485.

JORDAN RW & PUDSEY CJ. 1992. High-Resolution Diatom Stratigraphy of Quaternary Sediments from the Scotia Sea. Mar Micropaleontol 19(3): 201-237. doi: 10.1016/0377-8398(92)90029-J.

KHIM BK, YOON HI, KANG CY & BAHK JJ. 2002. Unstable Climate Oscillations during the Late Holocene in the Eastern Bransfield Basin, Antarctic Peninsula. Quat Res 58(3): 234-245. doi: 10.1006/qres.2002.2371.

KLAJA J & DUDEK L. 2016. Geological Interpretation of Spectral Gamma Ray (SGR) Logging in Selected Boreholes. Nafta-Gaz 72. doi: 10.18668/NG2016.01.01.

KÜHNEL RA. 1996. Tonminerale Und Tone. Struktur, Eigenschaften, Anwendung and Einsatz in Industrie Und Umwelt: JASMUND K AND LAGALY G (Eds). Steinkopf Verlag, Darmstadt, 1993. Xiv+. ISBN 3-7985-0923-9, p. 490. doi: 10.1016/0169-1317(96)90003-4.

LAWVER LA, SLOAN BJ, BARKER DH, GHIDELLA M, VON HERZEN RP, KELLER RA, KLINKHAMMER GP & CHIN CS. 1996. Distributed, Active Extension in Bransfield Basin Antarctic Peninsula: Evidence from Multibeam Bathymetry. GSA Today. doi: 10.1130/GSAT01707GW.1.

LEITÃO FJ, NETO AA & VIEIRA R. 2016. Morphological and sedimentary characterization through analysis of multibeam data at Deception Island, Antarctic. Rev Bras Geof 34(2): 155-164. doi: 10.22564/rbgf.v34i2.792.

LEVENTER A, DOMACK EW, ISHMAN SE, BRACHFELD S, MCCLENNEN CE & MANLEY P. 1996. Productivity Cycles of 200-300 Years in the Antarctic Peninsula Region: Understanding Linkages among the Sun, Atmosphere, Oceans, Sea Ice, and Biota. GSA Bulletin 108(12): 1626-1644. doi: 10.1130/0016-606(1996)108<1626:PCOYIT>2.3.CO;2.

LEVENTER A, DOMACK EW, PIKE J, STICKLEY C, MADDISON E, BRACHFELD SA, MANLEY P & MCCLENNEN CE. 2006. Marine Sediment Record from the East Antarctic Margin Reveals Dynamics of Ice Sheet Recession. GSA Today. doi: 10.1130/GSAT01612A.1.

MARSHALL MC. 1975. Summary of Physical Properties. In Initial Reports of the Deep Sea Drilling Project. Vol. 32. U.S. Government Printing Office, p. 961-962.

MILLIKEN KT, ANDERSON JB, WELLNER JS, BOHATY SM & MANLEY PL. 2009. High-Resolution Holocene Climate Record from Maxwell Bay, South Shetland Islands, Antarctica. GSA Bulletin 121(11-12): 1711-1725. doi: 10.1130/B26478.1.

MUNSELL AH. 1992. Munsell Book of Color: Matte Finish Collection.

NIELSEN BL, LØVBORG L, SØRENSEN P & MOSE E. 1987. Gamma-Ray Analysis for U, Th, and K on Bulk Cutting Samples from Deep Wells in the Danish Subbasin and the North German Basin. Risø National Laboratory, DK-4000 Roskilde, Denmark. Report Risø-M-2646, 85.

NOBRE JA, FREIRE AFM, NETO AA, DOS SANTOS MARTINS M, SILVA CG, VIEIRA R. 2020. Quaternary warming and cooling trends in the Bransfield Basin, Antarctic Peninsula, based on gamma-ray spectrometry. Geo-Mar Let 40: 781-788. doi:10.1007/s00367-020-00658-4.

PRIETO MJ, CANALS M, ERCILLA G & DE BATIST M. 1998. Structure and Geodynamic Evolution of the Central Bransfield Basin (NW Antarctica) from Seismic Reflection Data. Mar Geol 149(1-4): 17-38. doi: 10.1016/S0025-3227(98)00038-3.

PRIETO MJ, ERCILLA G, CANALS M & DE BATIST M. 1999. Seismic Stratigraphy of the Central Bransfield Basin (NW Antarctic Peninsula): Interpretation of Deposits and Sedimentary Processes in a Glacio-Marine Environment. Mar Geol 157(1-2): 47-68. doi: 10.1016/S0025-3227(98)00149-2.

RĂDAN SC, RĂDAN S & CATIANIS I. 2013. The Use of the Magnetic Susceptibility Record as a Proxy Signature for the Lithological Composition of Lake Sediments: Evidences from Short Cores in the Meşteru - Fortuna Depression (Danube Delta). Geo-Eco-Marina 19(19): 77-106. doi: 10.5281/zenodo.56845.

ROCHA-CAMPOS AC & SANTOS PR. 2000. Ação Geológica Do Gelo. In: TEIXEIRA W, TOLEDO MCM, FAIRCHILD TR & TAIOLI F (Organiz). Decifrando a Terra. São Paulo, 568 p.

SANGRÀ P ET AL. 2011. The Bransfield Current System. Deep-Sea Res I 58: 390-402. doi: 10.1016/j.dsr.2011.01.011.

SCHULZ HD & ZABEL M. 2013. Marine Geochemistry. Springer Berlin Heidelberg.

SMITH WO & NELSON DM. 1985. Phytoplankton Bloom Produced by a Receding Ice Edge in the Ross Sea: Spatial Coherence with the Density Field. Science 227(4683): 163-166. doi: 10.1126/science.227.4683.163.

TRUSEL LD, POWELL RD, CUMPSTON RM & BRIGHAM-GRETTE J. 2010. Modern Glacimarine Processes and Potential Future Behaviour of Kronebreen and Kongsvegen Polythermal Tidewater Glaciers, Kongsfjorden, Svalbard. Geol Soc Spec Publ 344(1): 89-102. doi: 10.1144/SP344.9.

VAUGHAN DG, MARSHALL GJ, CONNOLLEY WM, PARKINSON C, MULVANEY R, HODGSON DA, KING JC, PUDSEY CJ & TURNER J. 2003. Recent Rapid Regional Climate Warming on the Antarctic Peninsula. Climatic Change 60(3): 243-274. doi: 10.1023/A:1026021217991.

WIGNALL PB & MYERS KJ. 1988. Interpreting Benthic Oxygen Levels in Mudrocks: A New Approach. Geology 16(5): 452-455. doi: 10.1130/0091-7613(1988)016<0452:IBOLIM>2.3.CO;2.

WINFREY MR & ZEIKUS JG. 1977. Effect of Sulfate on Carbon and Electron Flow during Microbial Methanogenesis in Freshwater Sediments. Appl Environ Microbiol 33(2): 275-281. doi: 10.1128/AEM.33.2.275-281.1977.

WOHLENBERG J. 1982. Seismo-Acoustic and Geoelectric Experiments within the Urach 3 Borehole. The Urach Geothermal Project. (Swabian Alb, Germany), p. 97-100.

YOON HI, HAN MW, PARK BK, OH JK & CHANG SK. 1997. Glaciomarine Sedimentation and Palaeo-Glacial Setting of Maxwell Bay and Its Tributary Embayment, Marian Cove, South Shetland Islands, West Antarctica. Mar Geol 140(3-4): 265-282. doi: 10.1016/S0025-3227(97)00028-5.

YOON HI, PARK BK, CHANG SK, HAN MW & OH JK. 1994. Depositional Environment of Near-Surface Sediments, King George Basin, Bransfield Strait, Antarctica. Geo-Mar Lett. doi: 10.1007/BF01204465.

YOON HI, PARK BK, KIM Y & KIM D. 2000. Glaciomarine Sedimentation and Its Paleoceanographic Implications along the Fjord Margins in the South Shetland Islands, Antarctica during the Last 6000 Years. Palaeogeogr Palaeoclimatol Palaeoecol 157(3-4): 189-211. doi: 10.1016/S0031-0182(99)00165-0.

SUPLEMENTARY MATERIAL

Tables SI, SII.

MATEUS DOS SANTOS MARTINS[1]
https://orcid.org/0000-0001-9128-0105

FABRICIO FERREIRA[1,2]
https://orcid.org/0000-0001-9811-4409

ARTHUR AYRES NETO[1]
https://orcid.org/0000-0002-2982-245X

ROSEMARY VIEIRA[1,2]
https://orcid.org/0000-0003-0312-2890

[1]Programa de Pós-Graduação em Dinâmica dos Oceanos e da Terra, Universidade Federal Fluminense (DOT-UFF), Instituto de Geociências, Av. Gal. Milton Tavares de Souza, s/n, Campus da Praia Vermelha, Boa Viagem, 24210-346 Niterói, RJ, Brazil

[2]Universidade Federal Fluminense/UFF, Instituto de Geociências, Laboratório de Processos Sedimentares e Ambientais (LAPSA), Av. Gal. Milton Tavares de Souza, s/n, Campus da Praia Vermelha, Boa Viagem, 24210-346 Niterói, RJ, Brazil

Correspondence to: **Mateus dos Santos Martins**
E-mail: marttmatt2@gmail.com

Author contributions

Mateus dos Santos Martins main author, responsible for acquiring and processing the data, discussing and writing this manuscript with the Fabricio Ferreira support, who contributed to the acquisition of sediment cores and also in the writing process. The authors Arthur Ayres Neto and Rosemary Vieira actively participated from the beginning to the end of the study with the samples planning and acquisition, data discussion and also in the final work review.